Flow-Induced β-Hairpin Folding of the Glycoprotein Ibα β-Switch

5 AUTHORS, INCLUDING:

Yanxin Liu
University of California, San Francisco
19 PUBLICATIONS **295** CITATIONS

SEE PROFILE

Gloria Cardenas-Jiron
University of Santiago de Chile (USACH), Sa…
68 PUBLICATIONS **947** CITATIONS

SEE PROFILE

Flow-Induced β-Hairpin Folding of the Glycoprotein Ibα β-Switch

Xueqing Zou,[†‡] Yanxin Liu,[‡§] Zhongzhou Chen,[‡§] Gloria Ines Cárdenas-Jirón,[¶] and Klaus Schulten[‡§*]

[†]School of Physics, Peking University, Beijing, China; [‡]Beckman Institute, [§]Department of Physics, University of Illinois, Urbana, Illinois; and [¶]Departamento de Ciencias Químicas, Facultad de Química y Biología, Universidad de Santiago de Chile, Santiago, Chile

ABSTRACT   Flow-induced shear has been identified as a regulatory driving force in blood clotting. Shear induces β-hairpin folding of the glycoprotein Ibα β-switch which increases affinity for binding to the von Willebrand factor, a key step in blood clot formation and wound healing. Through 2.1-μs molecular dynamics simulations, we investigate the kinetics of flow-induced β-hairpin folding. Simulations sampling different flow velocities reveal that under flow, β-hairpin folding is initiated by hydrophobic collapse, followed by interstrand hydrogen-bond formation and turn formation. Adaptive biasing force simulations are employed to determine the free energy required for extending the unfolded β-switch from a loop to an elongated state. Lattice and freely jointed chain models illustrate how the folding rate depends on the entropic and enthalpic energy, the latter controlled by flow. The results reveal that the free energy landscape of the β-switch has two stable conformations imprinted on it, namely, loop and hairpin—with flow inducing a transition between the two.

INTRODUCTION

Proteins usually adopt a single three-dimensional structure after synthesis of their peptide chain. How a protein acquires its stably folded and functional structure from a linear peptide chain has been studied for decades (1,2). However, the folding landscape can have more than one structure imprinted on it as major domains of attraction, with one being more stable under some conditions and the others possibly more stable under variant conditions. In this case, protein structures are malleable by external factors and, indeed, proteins through change of their structures act as sensors of environmental properties like flow, light, ion concentration, or mechanical force (3–9). For example, a light-switchable peptide was reported to transform with light pulses from a β-hairpin to an unfolded state and vice versa (10). Another example is the muscle protein titin, which contains a kinase as a tension-sensor: mechanically induced sequential unfolding of titin kinase activates ATP binding, a response that controls muscle growth (11). Protein sensors also include voltage-gated potassium channels, involving transmembrane domains that open and close the channels in response to changes in transmembrane potential (12–14).

This study focuses on another protein malleable by a weak perturbation, namely, by blood flow, the flow inducing a secondary structure transition from a disordered loop to an ordered β-hairpin. The transition occurs in the β-switch region of glycoprotein Ibα (GPIbα) that initiates blood clotting when detecting bleeding-induced flow. As an important self-healing mechanism in higher organisms, blood clotting occurs almost instantly after blood vessel injury and bleeding onset. Blood clotting involves the coagulation of blood platelets around a wound. The interaction between platelet-receptor GPIbα and the von Willebrand factor

(vWF), a multimeric glycoprotein existing in blood plasma, contributes to platelet aggregation (15,16). Indeed, vWF binding to GPIbα is enhanced under flow conditions caused by blood vessel injury and bleeding (17).

The interaction of vWF and GPIbα is mediated by the A1 domain of vWF and the GPIbα subunit (18). Two sites on GPIbα that interact with the A1 domain of vWF were identified, namely, a β-hairpin at the N-terminus and a flexible loop at the C-terminus (19,20). The resolved crystal structures of GPIbα (Protein DataBank codes 1QYY and 1SQ0) showed that its C-terminal region adopts an ordered β-hairpin conformation when binding to the vWF, whereas without such binding, it adopts a disordered loop conformation (21,22). Accordingly, we refer in the following to the C-terminal region of GPIbα as the "β-switch". The structures suggest that β-hairpin folding of the β-switch increases the affinity of GPIbα binding to vWF (23).

It was proposed that blood flow, arising in the case of blood vessel damage and subsequent bleeding, induces β-hairpin folding in GPIbα and, thereby, enhances the binding of GPIbα to vWF (24). Molecular dynamics (MD) simulation, a useful tool to explore nanoscale biological processes in atomic-level detail (25–27), validated this hypothesis (24). In a previous study, we had employed molecular dynamics simulations to explore the loop $\rightarrow$ β-hairpin transition and had illustrated that the transition involves two consecutive steps—backbone rotation and side-group packing (28). However, the thermodynamics and kinetics of this β-hairpin folding in flow had not been characterized.

Other prior studies identified three general steps in β-hairpin folding, namely, hydrophobic collapse, turn formation, and interstrand hydrogen-bond formation. However, which step initiates the folding is still under debate (29–36). The "hydrophobic collapse" mechanism suggests that early hydrophobic cluster formation nucleates the β-hairpin folding (29), whereas the "zipper" mechanism

suggests that nucleation is initiated by turn formation, and followed by subsequent hydrophobic interactions (30). In addition, a "broken-zipper" mechanism, in which long-range hydrophobic interactions form more readily than the short-range ones, has been observed recently (36). In our study, the GPIbα β-switch offers a very small, namely, 17-amino-acids-long, oligopeptide sensor system on which flow-induced β-hairpin folding can be studied readily and in detail.

In this study, we performed 60 simulations of the GPIbα β-switch with different starting conformations and flow velocities that provided us with sufficient data to confirm the earlier characterization of the process and to investigate β-hairpin folding in more detail. In total, the simulations covered a 2.1-μs time period. We observed how flow-induced folding of the GPIbα β-hairpin combines hydrophobic collapse, interstrand hydrogen bonding, and turn formation. Adaptive biasing force (ABF) simulations (37–39) determined how flow changes the free energy landscape of the β-switch, revealing that flow stabilizes the β-switch in an elongated state, destabilizing the random loop state. Simulations were complemented through a theoretical analysis that explains the stabilization.

METHODS

We conducted several different types of simulations to study β-hairpin folding of the GPIbα β-switch. Sixty MD simulations at various flow conditions established the β-hairpin folding rate and its flow-velocity dependence. A 20-ns equilibration tested the thermal stability of the folded β-hairpin without flow. Twelve ABF simulations provided the potential of mean force for elongating the β-switch. A coarse-lattice model and a freely jointed chain model of the β-switch were considered to characterize the entropy-enthalpy balance effect on β-hairpin folding.

Simulated systems

Atomic coordinates of the β-switch, which consists of 17 residues (VYVWKQGVDVKAMTSNV), were taken from the GPIbα structure (Protein DataBank code 1QYY) (22), as shown in Fig. 1, truncating residues 227–243. To add missing hydrogen atoms and generate the protein structure file, we employed the psfgen plugin of VMD (40) with the topology file of CHARMM27 (41). The generated β-switch was placed into a water box of dimension 60 Å × 30 Å × 30 Å. One chloride ion was added to neutralize the system. The entire simulated system contained 9410 atoms.

At thermal equilibrium, the β-switch is a flexible loop and adopts a large number of conformations (28). Flow-induced β-hairpin folding can start from any of these conformations. In this study, we selected 20 different starting conformations and subjected them to flow at different velocities, namely, 0 m/s, 25 m/s, and 50 m/s. The starting conformations were obtained by first equilibrating the β-switch for 9 ns, then continuing the simulation and selecting a conformation every 1 ns. Flow was generated along the x axis, as described previously (28). Fig. S1 in the Supporting Material shows the flow velocity generated by this procedure.

Molecular dynamics

Simulations were performed with the program NAMD 2.6 (42), the CHARMM27 force field with CMAP corrections for the protein and ions
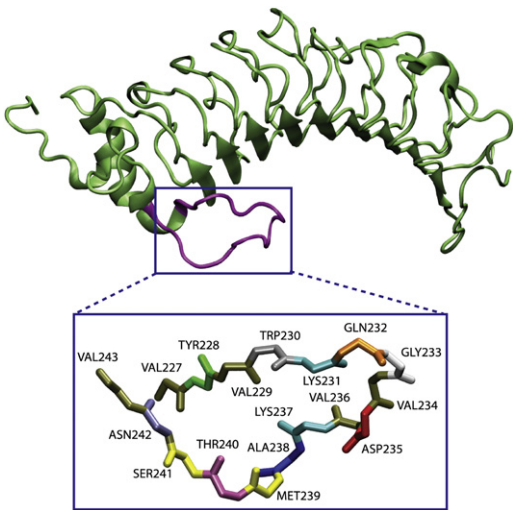

FIGURE 1 Structure of the α-subunit of GPIb. The mauve part is the β-switch region of GPIbα which has been simulated. The β-switch region contains 17 residues.

(41), and the TIP3P water model (43). Periodic boundary conditions and particle-mesh Ewald summation were employed. The integration timestep was 1 fs. The temperature was kept at 310 K by a Langevin thermostat with damping coefficient $\gamma = 0.1$ ps^{-1} (44). The C_α atoms of residues Val^{227}, Tyr^{228}, Ser^{241}, Asn^{242}, and Val^{243}, located at the β-switch ends, were constrained by a harmonic potential with a spring constant of 1 (kcal/mol) Å^{-2}. Twenty 25-m/s-flow simulations covered 60 ns of simulation, whereas twenty 50-m/s-flow simulations and twenty 0-m/s-flow simulations covered only 20 ns, because statistics had converged sufficiently at this point in time. Altogether, we carried out 2.1 μs of simulations, all listed in Table 1.

Adaptive biasing force

To measure how flow, in inducing β-hairpin formation, alters the transition path energetics, we carried out three sets of ABF simulations (37–39) under flow conditions with 0 m/s, 25 m/s, and 50 m/s velocities. The coordinate sampled by the ABF simulations was the distance, δ, between the

TABLE 1   List of simulations

Name	Type	Flow velocity	δ-interval	Time (ns)
A1–A20	EQ	0 m/s	—	20
B1–B20	EQ	25 m/s	—	60
C1–C20*	EQ	50 m/s	—	20
D	EQ	0 m/s	—	20
E1	ABF	0 m/s	10–13 Å	3
E2	ABF	0 m/s	13–18 Å	5
E3	ABF	0 m/s	18–23 Å	5
E4	ABF	0 m/s	23–28 Å	5
F1	ABF	25 m/s	10–13 Å	3
F2	ABF	25 m/s	13–18 Å	5
F3	ABF	25 m/s	18–23 Å	5
F4	ABF	25 m/s	23–28 Å	5
G1	ABF	50 m/s	10–13 Å	3
G2	ABF	50 m/s	13–18 Å	5
G3	ABF	50 m/s	18–23 Å	5
G4	ABF	50 m/s	23–28 Å	5

EQ, equilibrium; ABF, adaptive biasing force.
*See Movie S1 and Movie S2, which show trajectory C1.

C_α atoms of the middle residue Asp^{235} and the final residue Val^{243}. The value δ represents the overall length of the extended β-switch. The sampling of δ was confined to the interval ranging from 10 Å to 28 Å. For each velocity, four consecutive ABF simulations were conducted to cover the entire δ-interval. The width of the sampling window covered in each ABF simulation (E1–E4, F1–F4, and G1–G4; see Table 1) was 5 Å, except for E1, F1, and G1, where the sampling window was 3 Å. The size for each ABF sampling bin was 0.1 Å.

Analysis of trajectories

To evaluate β-hairpin folding kinetics, we first define the folded structure state. Five established hydrogen bonds (229HN-240O, 240HN-229O, 231HN-238O, 238HN-231O, and 233HN-236O) are deemed characteristic for the fully folded β-hairpin, as shown in Fig. S2 a. A hydrogen bond is considered formed when the distance between acceptor atom and donor atom is <3.0 Å. Because the C_α atoms of residues Val^{227}, Tyr^{228}, Ser^{241}, Asn^{242}, and Val^{243} are constrained, we define the length of the β-switch as the distance between 241CA and 235CA (Fig. S2 b). A water molecule is recognized as interstrand when the condition $r_{water,\beta-switch} < R_{interstrand}$ is met, where $r_{water,\beta-switch}$ is the distance between water molecule and the β-switch, and $R_{interstrand}$ is the maximal distance among five defined hydrogen bonds. The secondary structure analysis of β-hairpin folding was performed using the Timeline plugin of VMD (40).

Lattice model

To characterize the entropy effect on flow-induced β-hairpin folding, we employed a coarse two-dimensional lattice model described through Monte Carlo simulation (45). In the model, the amino acids of the β-switch are represented by beads, the C_α atoms representing the bead position in our model, i.e., the C_α trace represents the conformation of the β-switch in the lattice model.

The basis vectors of the lattice model are (2, 1) and (1, 2), such that every bead has eight neighbors, as shown in Fig. S6. The valence angles in the C_α trace are restricted to the range (90°, 126.8°). The spacing of the lattice is 1.7 Å, the distance of a pair of neighboring beads measuring then 3.8 Å (45).

In the lattice model, we considered only a sequence-independent statistical potential for a C_α trace conformation, $E_{C_\alpha-trace}$ (45). The total energy of the model β-switch is

$$E = E_{C_\alpha-trace} + E_{H-bond} + E_{flow}. \qquad (1)$$

Here E_{H-bond} is an additional potential accounting for hydrogen-bond formation (45), and E_{flow} represents a flow effect taken into account through a dragging force acting on each bead. We applied three sample forces, 0 pN, 10 pN, and 20 pN, all pointing in the x direction. The Monte Carlo simulations started from the same random self-avoiding conformation. Each Monte Carlo step selected a random conformational change as the next move, using a Metropolis criterion to accept or reject the proposed move (46,47).

The conformation of the β-switch is described by the sequence of lattice points occupied by each C_α atom. The length of the chain is defined as the distance between the first and the middle (the 8th) C_α atoms.

Freely jointed polymer model

The model used contains, for zero flow, no enthalpic contribution whatsoever, attributing the same energy ($E = 0$) to all conformations of the β-switch. In this model, the β-switch is represented by a polymer of 17 units, each unit corresponding to one amino acid. For the purpose of this description, we ascribe δ again to the distance between the beginning of unit 1 and the end of unit 8 as well as to the distance from the beginning of unit 9 to the end of unit 17. The amino acid backbone units, each described by a vector

$\vec{r}_j, j = 1, 2, ...17$, are assumed freely jointed, i.e., the orientations of any two units are uncorrelated as

$$\langle \vec{r}_j \cdot \vec{r}_k \rangle = 0, j \neq k.$$

The length of each unit is $a = 3.9$ Å (the distance between the C_α atoms of adjacent residues), i.e.,

$$\langle \vec{r}_j \cdot \vec{r}_j \rangle = a^2.$$

Because the two ends (i.e., $j = 1$ and $j = 17$) of the β-switch are constrained next to each other, it must hold $\sum_{j=1}^{17} \vec{r}_j = 0$ and, hence,

$$\sum_{j=1}^{8} \vec{r}_j = -\sum_{j=9}^{17} \vec{r}_j \qquad (2)$$

or $\delta = |\sum_{j=1}^{8} \vec{r}_j| = |\sum_{j=9}^{17} \vec{r}_j|$.

Let us assume, currently, that $\vec{R}_1 = \sum_{j=1}^{8} \vec{r}_j$ is independent of $\vec{R}_2 = \sum_{j=9}^{17} \vec{r}_j$. For the distribution of $\vec{R}_1$ holds according to well-known freely jointed chain theory (48)

$$P_1(\vec{R}_1) = (3/2\pi N_1 a^2)^{3/2} \exp(-3R_1^2/2N_1 a^2), \qquad (3)$$

where $N_1 = 8$. For $P_2(\vec{R}_2)$, an analogous expression holds with $N_2 = 9$. Condition Eq. 2 implies that in the case of the β-switch, we have $\vec{R}_1 = -\vec{R}_2$. From this, one can conclude that $\vec{\delta}$ defined through $\vec{\delta} = \sum_{j=1}^{8} \vec{r}_j$ and represented through spherical coordinates $\vec{\delta} = (\delta, \theta, \phi)$ obeys the distribution

$$Q(\vec{\delta}) = P_1(\vec{\delta})P_2(-\vec{\delta}) / \int_0^\infty \delta^2 \, d\delta \int_0^\pi \sin\theta \, d\theta \\ \times \int_0^{2\pi} d\phi P_1(\vec{\delta})P_2(-\vec{\delta}). \qquad (4)$$

One can readily derive, using Eq. 3,

$$Q(\vec{\delta}) = \left[3(N_1 + N_2)/2\pi a^2 N_1 N_2\right]^{3/2} \\ \times \exp\left(-3(N_1 + N_2)\delta^2/2N_1 N_2 a^2\right). \qquad (5)$$

This distribution corresponds to the free energy

$$U(\vec{\delta}) = -k_B T \ln Q(\vec{\delta}). \qquad (6)$$

We consider now the enthalpic effect due to flow. In the case of flow, each amino acid unit is assumed to be subject to a force $\vec{f}$ arising from the flow. In describing the effect of the flow, we assume that the flow rotates and shapes the β-switch such that the endpoint of amino acid 8 forms the tip of the β-switch. Amino acids $j = 1,...8$ then experience an interaction $-\vec{f} \cdot \vec{r}_j$, whereas amino acids $j = 9,...17$ experience an interaction $+\vec{f} \cdot \vec{r}_j$ (i.e., the first eight amino acids are induced to point parallel to the flow, whereas the next nine amino acids are induced to point antiparallel to the flow). We note that flow, in principle, should favor equally, at the low resolution of our simple model, any polymer segment that is parallel or antiparallel to the flow. Condition Eq. 2 implies then that the overall interaction is

$$W_{flux}(\vec{\delta}) = -2\vec{f} \cdot \vec{\delta}.$$

One can conclude that the $\vec{\delta}$ distribution, $\tilde{Q}(\vec{\delta})$, in the presence of flow, is

$$\tilde{Q}(\vec{\delta}) = Z' \, Q(\vec{\delta})\exp\{-W_{flux}(\vec{\delta})/k_B T\}, \qquad (7)$$

where Z' is a normalization factor defined through

$$\int_{\Omega} d\vec{\delta}\, \tilde{Q}(\vec{\delta}) = 1,$$

where $\tilde{Q}(\vec{\delta})$ as given by Eq. 7, like $Q(\vec{\delta})$, is a Gaussian distribution with the same standard deviation as $Q(\vec{\delta})$, but with flow changing the mean of $\tilde{Q}(\vec{\delta})$. An analysis, given in the Supporting Material, shows that displacement of the mean, for a flow in the x direction characterized through force f, is

$$\Delta x = (2fa/3k_BT)[N_1N_2/(N_1 + N_2)]a. \tag{8}$$

RESULTS

This section is based on the simulations (listed in Table 1) of β-hairpin folding of the β-switch region of GPIbα. We examine first the time evolution of β-hairpin folding and establish the rate of the loop $\rightarrow$ β-hairpin transition. We then characterize the folding kinetics of β-hairpin folding under different flow velocities. ABF simulations were conducted to calculate the free energy between loop state and elongated state of the β-switch. Finally, a coarse two-dimensional lattice model and a freely jointed chain model are invoked to describe the flow-dependent entropy-enthalpy balance in β-hairpin folding.

Time evolution of β-hairpin folding

Sixty simulations were carried out to investigate β-hairpin folding under different flow conditions. Fig. 2 shows the time evolution of twenty 60-ns simulations with 25 m/s-flow and twenty 20-ns simulations with 50 m/s-flow. Under 25 m/s flow, β-hairpin folding completed in five trajectories (B4, B10, B14, B16, and B18) during 60 ns simulation time, whereas under 50 m/s-flow, 10 trajectories (C1, C2, C4, C5, C9, C10, C12, C13, C14, and C16) showed β-hairpin folding during 20 ns. Obviously, β-hairpin formation occurs spontaneously under strong enough flow. Fig. S3 shows histograms of the β-switch length distribution and of interstrand hydrogen-bond formation for flow velocities of 0 m/s, 25 m/s, and 50 m/s in 20 ns. At zero velocity, the length of the β-switch fluctuated at ~12 Å, and no hydrogen bonds formed. However, for flows of 25 m/s and 50 m/s the average extension was 18 Å and 20 Å, respectively—indicating that the β-switch prefers to adopt an elongated conformation under flow, whereas it prefers a loop confor-

mation without flow. In the simulations, the β-switch often did not form a complete β-hairpin, i.e., one containing all five possible hydrogen bonds; instead, a partial β-hairpin containing only 2–4 hydrogen bonds often formed at 25 m/s-flow and 50 m/s-flow. As shown in Fig. S3 b, in 20 ns, for 25 m/s flow, 70% β-switches formed 3–5 hydrogen bonds, whereas for 50 m/s-flow, 80% β-switches formed 4–5 hydrogen bonds.

Flow velocity-dependence of hairpin-folding kinetics

Flow exerts a dragging force on the β-switch and causes backbone dihedrals to rotate in the direction that increases the length of the β-switch and benefits interstrand hydrogen bonding, as shown in Fig. S4. For each flow velocity, we calculated the distribution of the β-switch length and number of interstrand hydrogen bonds using all 20 trajectories. Fig. 3 a shows how the speed of extension of the β-switch increases with flow velocity. For flow at 50 m/s velocity, the average length of the β-switch increased to 20.5 Å in 10 ns; for flow at 25 m/s velocity, its average length reached 18.5 Å at ~20 ns and kept increasing slowly over the next 40 ns. Without flow, the average length fluctuated at ~13 Å, which implies that the β-switch remained in a loop conformation. Movie S1 shows how flow-induced backbone rotation is linked to β-switch extension.

The interstrand hydrogen-bond formation seen in our simulations is consistent with the extension of the β-switch under different flow velocities. As shown in Fig. 3 b, the speed of hydrogen-bond formation increased with faster flow. The average number of hydrogen bonds increased within 20 ns, from 0 to 3.2, under a 50 m/s flow. Flow at 25 m/s yielded, on average, in 20 simulations, only two hydrogen bonds per trajectory during the first 20 ns. During the next 40 ns, the average number of hydrogen bonds increased to 3.2.

Folding mechanism

Backbone rotation and side-chain packing are two steps involved in β-hairpin folding as demonstrated for the β-switch before (28) and for β-hairpin folding in general (35), but the key factor initiating β-hairpin folding is still
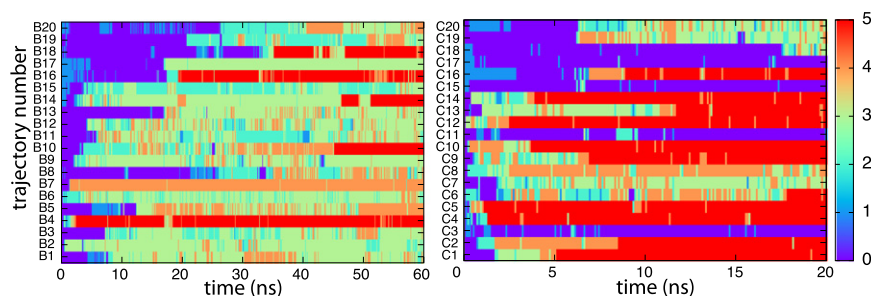

FIGURE 2 Time evolution of interstrand hydrogen-bond formation under 25 m/s-flow and 50 m/s-flow. Colors indicate the number of interstrand hydrogen bonds established (see *color bar* on *right*). The 25 m/s-flow (*left*) induced five β-hairpin foldings in 60 ns (B4, B10, B14, B16, and B18). The 50 m/s-flow (*right*) induced 10 β-hairpin foldings in 20 ns (C1, C2, C4, C5, C9, C10, C12, C13, C14, and C16).
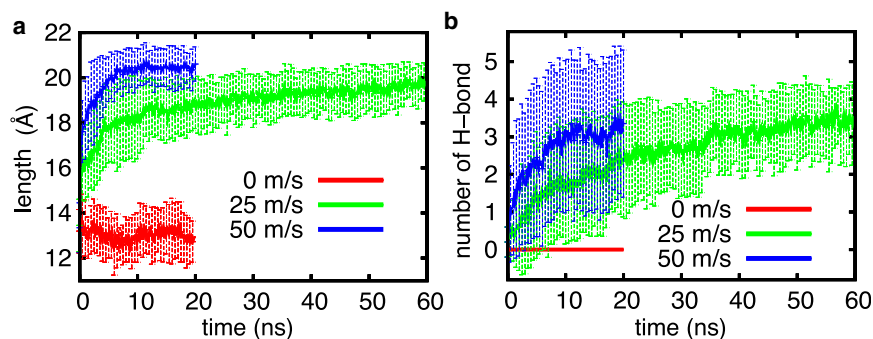
FIGURE 3 Flow velocity-dependent β-switch extension and interstrand hydrogen-bond formation. (*a*) Extension of the β-switch under 0 m/s flow, 25 m/s flow, and 50 m/s flow. (*b*) Different rate of interstrand hydrogen-bond formation. For each velocity, 20 trajectories were used to calculate mean value and deviation. See Movie S1 and Movie S2, which show the β-switch extension and β-hairpin formation.

under debate (31,34). In case of the GPIbα β-switch, the ends of the β-switch are constrained by other parts of the protein, and its folding mechanism may be different from that of free β-hairpins. To elucidate flow-induced β-hairpin folding of the β-switch, we analyzed the formation of the hairpin turn and the formation of interstrand hydrogen bonds as well as the side-chain packing of key residues.

There are four residues (Gly[233], Val[234], Asp[235], and Val[236]) involved in the turn formation, and three pairs of residues (Val[229]-Thr[240], Lys[231]-Ala[238], and Gly[233]-Val[236]) establish five interstrand hydrogen bonds (Fig. S2 *a*). As shown

in Fig. 4, during a 50 m/s flow, the side-chain packing happened first and was followed by interstrand hydrogen-bond formation and G233-V234-D235-V236 (GVDV) turn formation. The folding pathway to the β-hairpin is similar in 10 trajectories: Side-chain packing of residues located at the open-end of the β-switch starts the folding process, with hydrogen bonds forming from left to right. The GVDV turn forms after side-chain packing is completed. The closed-end hydrogen bond (236O-233HN) becomes established after GVDV turn formation, for the last step of β-hairpin completion. During a 25 m/s flow, five simulations
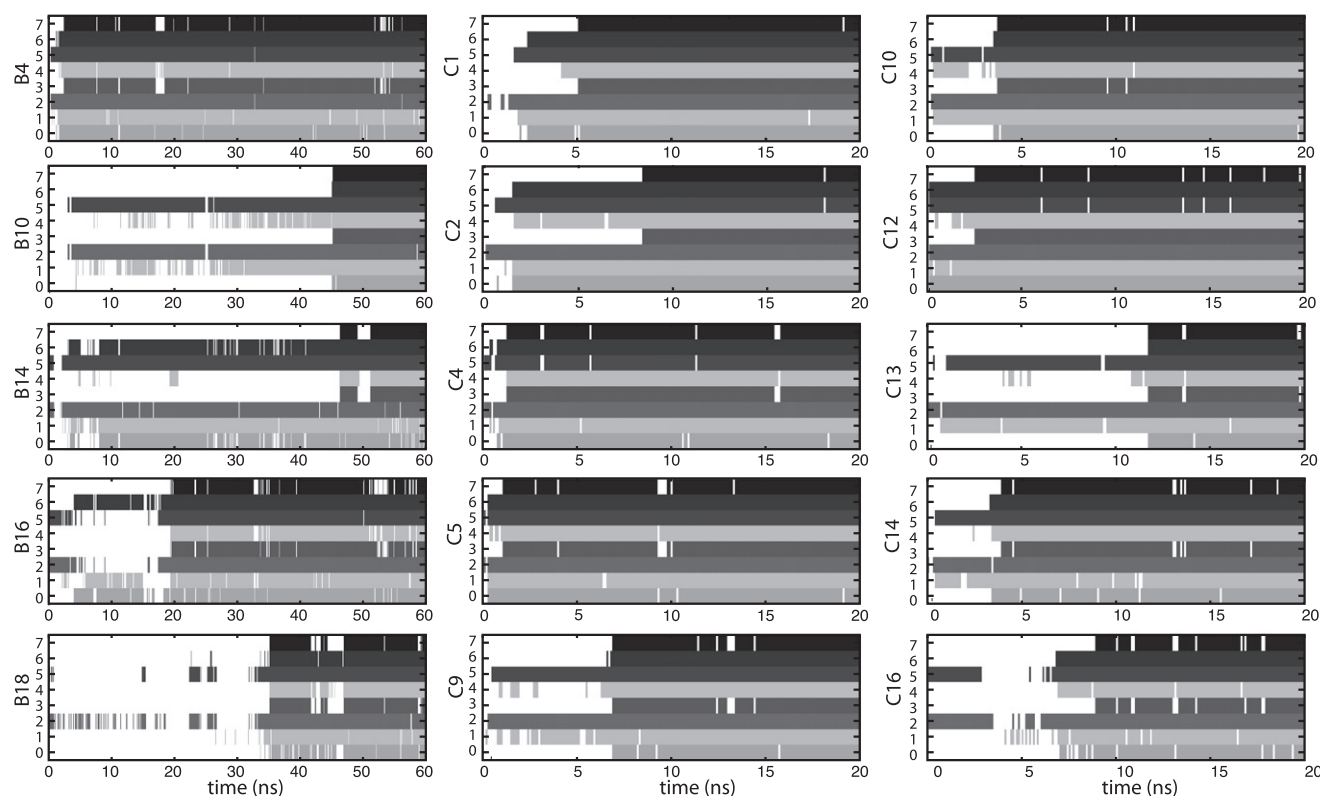

FIGURE 4 Progress in β-hairpin folding under 25 m/s flow and 50 m/s flow. Shown is the analysis of simulations at 25 m/s-flow (*left*) and 50 m/s-flow (*middle*, *right*). The properties represented by each row are: (*0*) native contact between residue Val[236] and Gly[233] (close to turn); (*1*) native contact between residue Ala[238] and Lys[231] (middle); (*2*) native contact between residue Thr[240] and Val[229] (close to the open end); (*3*) hydrogen bond 236O-233HN (close to turn); (*4*) hydrogen bond 238HN-231O (middle); (*5*) hydrogen bond 240O-229HN (close to the open end); (*6*) turn formation; and (*7*) five established interstrand hydrogen bonds (folded β-hairpin). Gray levels are used only to differentiate (*0*)-(*7*) properties.

(i.e., B4, B10, B14, B16, and B18) showed a similar folding pathway. Movie S2 shows a typical flow-induced β-hairpin folding trajectory.

Secondary structure throughout 15 β-hairpin folding trajectories presented in Fig. S5 shows a similar order of events along the folding pathway: the interstrand hydrogen bonds formed from the open-end to the closed-end of the β-switch. The turn was formed before the establishment of the closed-end hydrogen bond. In some simulations, instead of the GVDV turn, another turn formed initially (for example, in simulations C9 and C13, one involving residue Lys[237]). This wrongly formed turn disturbed interstrand hydrogen-bond formation until, eventually, the correct GVDV turn formed that permitted completion of β-hairpin folding. In all trajectories, the GVDV turn was stable after its formation.

Interstrand water molecules

Water plays a major role in modulating the weak interactions in biological systems. In the case of β-hairpin folding, before the hydrogen-bond acceptor and donor from each chain approach each other, water molecules interact with the respective polar atoms, hindering interstrand hydrogen-bond formation. When the β-switch adopts a loop state, the area between interstrands is large enough to permit a number of water molecules to be in contact with polar atoms, as shown in Fig. 5, a and b. Under flow conditions, the β-switch is stretched in the direction of the flow, and as a result, the interstrand area becomes small, such that only a few water molecules can permeate through the interstrand area, as shown in Fig. 5, c and d. In Fig. 5, e and f, no interstrand water molecule is observed in a folded β-hairpin.

To demonstrate the change in the number of interstrand water molecules when the β-switch undergoes its conformational transition, we chose five typical trajectories for analysis. As shown in Fig. 5 g, without flow, the number of interstrand water molecules fluctuates at ~20. With flow, the number of interstrand water molecules drops significantly after the β-switch becomes stretched. In case of a fully folded β-hairpin, no interstrand water molecule remains. Movie S3 shows how the number of water molecules drops during the β-hairpin folding process.

Thermal stability of folded β-hairpin

In our simulations, β-hairpins induced by flow remained stable under the assumed flow conditions during simulation time. To find out whether the flow is necessary for maintaining the folded β-hairpin, we removed the flow after β-hairpin folding was complete, and continued the simulation for another 20 ns. Without flow, the backbone of the β-switch was no longer stretched, yet its length did not decrease (as shown in Fig. 6). Hydrogen bonds remained stable, except for one hydrogen bond (233HN-236O) that
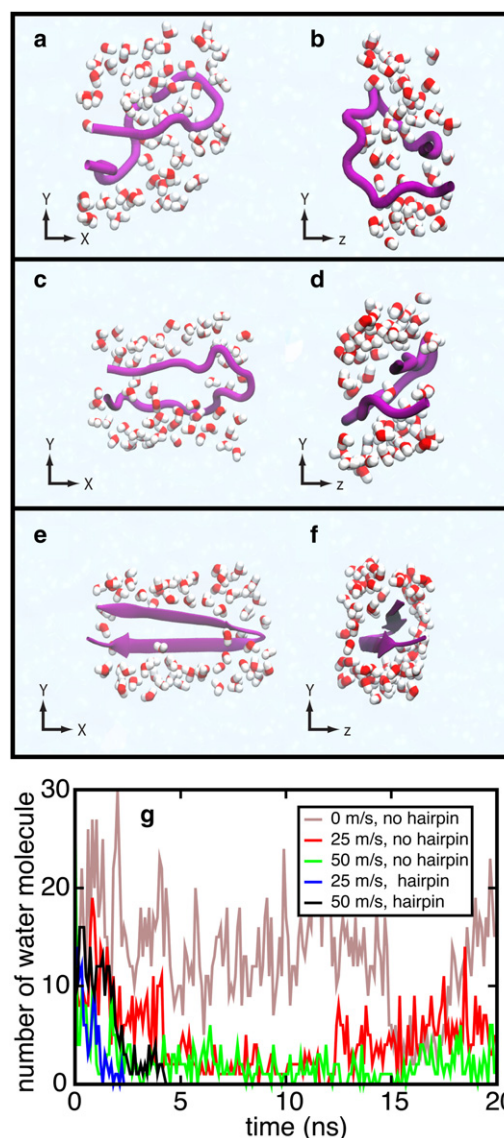

FIGURE 5 Snapshots of water molecules surrounding the β-switch and number of water molecules between strands of the β-switch in five selected simulations. (a and b) In the loop state, the two strands of the β-switch, shown in purple, are separated by a number of water molecules. (c and d) In an elongated nonhairpin state, the number of water molecules between the two strands is reduced, but a few water molecules remain present. (e and f) No water molecule remains between the two strands in a folded β-hairpin. (g) Change of water molecules in five selected simulations, in which the β-switch adopts three different conformations: random loop (brown), elongated loop (red and green), and folded β-hairpin (blue and black). See Movie S3, which shows the interstrand water molecules.

became temporarily broken for 4 ns. According to a secondary structure analysis, the β-hairpin remained stable for most of the 20 ns. The fluctuation of the hydrogen bond (233HN-236O) caused a temporary unfolding at the closed-end of the β-hairpin. When this hydrogen bond (233HN-236O) was broken, the GVDV turn also disappeared. The observation that the open-end of β-hairpin forms more readily and is more stable than the closed-end
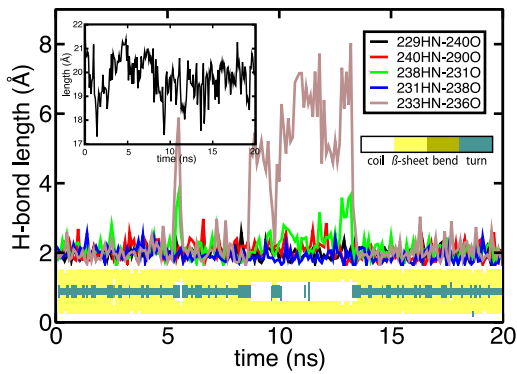
FIGURE 6 Dynamics of a flow-induced β-hairpin when flow is switched off. (*Inset*, *left*) Length of the β-switch. (*Bottom*) The secondary structure.

was also made by Lewandowska et al. (36). However, even when thermal fluctuation induced partial unfolding of the β-hairpin, the β-switch restored the fully folded β-hairpin spontaneously without flow.

Free energy barrier of β-hairpin formation

To investigate how flow influences the free energy landscape for β-switch extension, we performed ABF simulations to calculate, for different flow velocities, the potential of mean force accounting for stretching the β-switch. The state of length $\delta = 10$ Å defined the reference energy $\Delta E = 0$.

Fig. 7 presents the free energy profiles for different flows. The free energy minimum for flow at 0 m/s velocity is -21 kcal/mol, which is located at 13 Å; for 25 m/s it is -24 kcal/mol located at 18 Å; and for 50 m/s velocity it is -27 kcal/mol located at 24 Å. The results shown in Fig. 7 exhibit three important features: 1), the free energy profile is clearly sensitive to the velocity of flow; 2), the position of the free energy minimum moves toward larger extension with increasing flow velocity; and 3), increased flow stabilizes the free energy minimum connected with the elongated β-switch conformation.
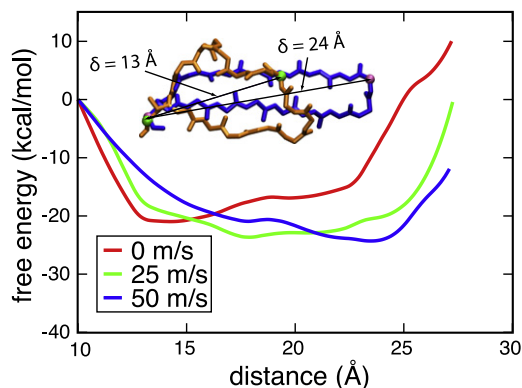

FIGURE 7 Potential of mean force profile for extending the β-switch from 10 Å to 28 Å at 0 m/s (*red*), 25 m/s (*green*), and 50 m/s (*blue*) flow velocity. (*Inset*, *top*) Two overlaid snapshots of the β-switch corresponding to free energy minima at zero (*orange*) and 50 m/s flow (*blue*).

Lattice model and freely jointed chain model

The flow-induced conformational change of the β-switch reflected in the free energy profile $\Delta G(\delta)$ (shown in Fig. 7) comes about through two main contributions, one entropic and the other enthalpic. The entropic energy contribution accounts for a large number of thermally accessible conformations for small δ-values in contrast to a small number for large δ-values. Entropy clearly favors small δ-values. The enthalpic contribution is due to flow that exerts forces extending the β-switch, and favors large δ-values. Here we consider two basic models capturing the two contributions, focusing solely on the entropic feature of the model. One is a coarse two-dimensional lattice model, which gives a straightforward picture of how flow changes the accessible conformational space of the β-switch. The other one is a freely jointed chain model, which provides a simple description of flow effect on stretching the β-switch. The combination of MD simulation, lattice model, and freely jointed chain model shows the external force effect on the entropy-enthalpy balance of the β-switch at three levels of resolution.

Fig. 8 *a* shows results obtained from the lattice model. The stretching force completely changes the accessible conformational space of the peptide chain. At zero force, the peptide chain adopts conformations symmetric at $x = 0$. When a force is applied, the preferred accessible conformational space is greatly reduced; only the conformations
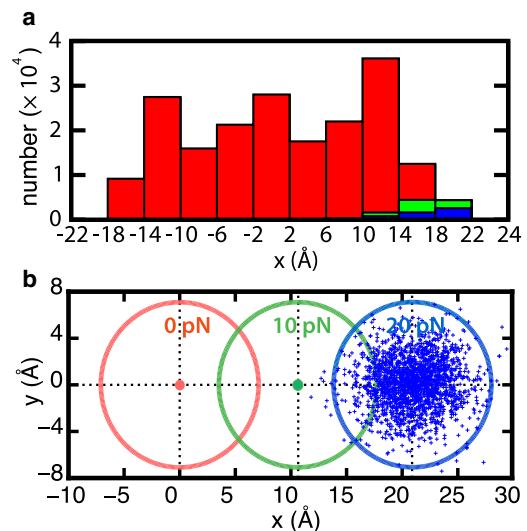

FIGURE 8 Results of two-dimensional lattice model and freely jointed chain model of the β-switch. (*a*) Force effect on the entropy of the β-switch as shown by the lattice model. The value x presents the x projection length of the peptide chain. (*b*) Tip-end distribution $Q(\overrightarrow{\delta})$ calculated from freely jointed chain model for zero flow (see Eq. 5) and $Q(\overrightarrow{\delta})$ (see Eq. 7) for flow described through forces $f = 10$ pN and $f = 20$ pN in the x, y plane, i.e., for $z = 0$. The mean displacement is given by Eq. 8. The circles circumscribe the spherical regions where the probability to find the tip of the β-switch is 90%. Random positions of the β-switch tip are shown for the 20 pN force case. Both models show that the enthalpic contribution stemming from flow changes the accessible conformational space of the β-switch and makes the elongated conformations more favorable.

extending far in the $+x$ direction are accessible. The magnitude of the force determines the average x-projection length of the conformation: under 10 pN force, the peptide chain adopts a length of 18 Å; and under 20 pN force, it adopts a length of 20 Å.

In the case of the freely jointed chain model, presented in Fig. 8 b, the distribution $\tilde{Q}(\vec{\delta})$ shifts, in the x, y plane at $z = 0$ under the effect of flow, from a zero flow average δ value of 0 Å to values of 11 Å and 21 Å for f equal to 10 pN and 20 pN, respectively. The average displacement of δ is predicted by Eq. 8. For each applied force, the circles shown in Fig. 8 b surround the spherical volume over which the total probability of tip placement is 90%. For the sake of illustration, we only show the distribution $\tilde{Q}(\vec{\delta})$ in the x, y plane. Admittedly, the model adopted here for the β-switch is very schematic, but it illustrates very well that the loop → β-hairpin transition of the β-switch involves a shift of balance between entropic and enthalpic energy contributions, which is consistent with the results of the lattice model.

DISCUSSION AND CONCLUSION

In this article, we have investigated a role of water flow on β-hairpin folding for the β-switch, a segment of the protein GPIbα that acts as a sensor for blood flow in wound healing. Simulations have demonstrated that during 25 m/s-flow and 50 m/s-flow, the β-switch folds readily into a β-hairpin, but does not do so without flow. Hence, the mechanism of the flow-induced folding has been identified.

This article corroborates and extends an earlier study on the flow-induced loop → β-hairpin transition of the β-switch (28). The importance of understanding the influence of environmental factors on protein folding, in the case of proteins acting as sensors in general, and of blood flow-sensing proteins in wound healing in particular, warrants a more detailed new investigation. The earlier study demonstrated through sets of ten 20-ns-long simulations at 50 m/s-flow (starting from two geometries) and one simulation at zero flow (for the wild-type β-switch) how backbone dihedral rotation extends the β-switch and alters the entropy-enthalpy balance such that flow renders the β-hairpin geometry more stable than the disordered loop ones. The new study extended the number of the wild-type β-switch MD simulations from 11 to 60, in particular, adding twenty 60-ns-long simulations under 25 m/s-flow condition because flow velocity of 50 m/s far exceeds natural blood speed. A new, advanced structure analysis of all 60 trajectories revealed further mechanistic details for the β-hairpin folding, in particular, side-group packing and hydrophobic collapse extruding interstrand water molecules at an early stage of the process.

A key new result is the potential of mean force for the extension of the β-switch. The potential, determined through ABF simulations (37–39) carried out at different flow speeds (0 m/s, 25 m/s, 50 m/s), shows a progressive stabilization of the β-hairpin geometry and a lowering of the free energy barrier separating loop and β-hairpin geometries. The change in energy can be attributed to a shift of the balance between entropic and enthalpic contributions. For this purpose, two models, a lattice model for the β-hairpin folding and a freely jointed chain model, demonstrate clearly that under flow conditions only conformations extending far in the flow-direction are accessible.

The findings can be summarized through the flow-dependent energy diagrams sketched in Fig. 9. A key feature here is that even under zero flow, loop form and β-hairpin form are stable. Although the β-hairpin form is only marginally stable, it does not readily unfold. This has been demonstrated in the new study through a zero-flow simulation of the β-switch in a β-hairpin state.

In summary, our study on flow-induced β-hairpin folding illustrates the role of external force on protein folding. Protein folding in biological cells is driven by many weak forces, some of which stem from within the protein, whereas some stem from the environment. From the environment, external factors such as pH value, temperature, pressure, and movement of water can influence folding. The β-switch of GPIbα adopts a loop conformation without flow, but once a blood vessel is injured, bleeding causes elongational flow (49,50) or turbulent flow. Shear then triggers the β-hairpin folding of the GPIbα β-switch; this conformational change increases the binding affinity of GPIbα to von Willebrand factor and eventually leads to blood clotting, which heals the vessel. Apparently, for the β-switch of GPIbα, the
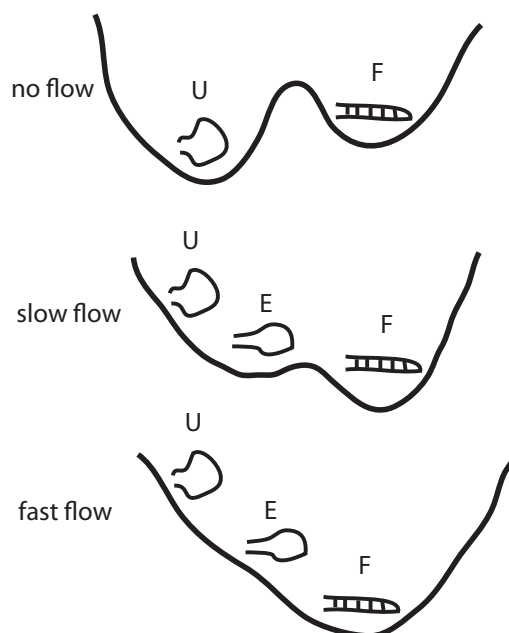

FIGURE 9 Schematic representation of the free energy landscape of the β-switch under different flow conditions. (*U*) Unfolded β-switch in loop state. (*F*) Folded β-hairpin. (*E*) Elongated β-switch.

laminar flow prevalent in a healthy blood vessel does not induce elongation. It is amazing how weak environmental effects along with a pluripotent free energy landscape can render a simple protein a highly sensitive detector.

SUPPORTING MATERIAL

Six figures, two equations, and three movies are available at http://www. biophysj.org/biophysj/supplemental/S0006-3495(10)00674-0.

REFERENCES

1. Montelione, G. T., and H. A. Scheraga. 1989. Formation of local structures in protein folding. *Acc. Chem. Res.* 22:70–76.

2. Onuchic, J. N., Z. Luthey-Schulten, and P. G. Wolynes. 1997. Theory of protein folding: the energy landscape perspective. *Annu. Rev. Phys. Chem.* 48:545–600.

3. Marszalek, P. E., H. Lu, …, J. M. Fernandez. 1999. Mechanical unfolding intermediates in titin modules. *Nature.* 402:100–103.

4. Bao, G., and S. Suresh. 2003. Cell and molecular mechanics of biological materials. *Nat. Mater.* 2:715–725.

5. DeMarco, M. L., and V. Daggett. 2005. Local environmental effects on the structure of the prion protein. *C. R. Biol.* 328:847–862.

6. Lou, J., T. Yago, …, R. P. McEver. 2006. Flow-enhanced adhesion regulated by a selectin interdomain hinge. *J. Cell Biol.* 174:1107–1117.

7. Saam, J., E. Tajkhorshid, …, K. Schulten. 2002. Molecular dynamics investigation of primary photoinduced events in the activation of rhodopsin. *Biophys. J.* 83:3097–3112.

8. Vogel, V. 2006. Mechanotransduction involving multimodular proteins: converting force into biochemical signals. *Annu. Rev. Biophys. Biomol. Struct.* 35:459–488.

9. Baldauf, C., R. Schneppenheim, …, F. Gräter. 2009. Shear-induced unfolding activates von Willebrand factor A2 domain for proteolysis. *J. Thromb. Haemost.* 7:2096–2105.

10. Schrader, T. E., W. J. Schreier, …, W. Zinth. 2007. Light-triggered β-hairpin folding and unfolding. *Proc. Natl. Acad. Sci. USA.* 104: 15729–15734.

11. Puchner, E. M., A. Alexandrovich, …, M. Gautel. 2008. Mechanoenzymatics of titin kinase. *Proc. Natl. Acad. Sci. USA.* 105:13385–13390.

12. Nishizawa, M., and K. Nishizawa. 2008. Molecular dynamics simulation of Kv channel voltage sensor helix in a lipid membrane with applied electric field. *Biophys. J.* 95:1729–1744.

13. Freites, J. A., D. J. Tobias, …, S. H. White. 2005. Interface connections of a transmembrane voltage sensor. *Proc. Natl. Acad. Sci. USA.* 102:15059–15064.

14. Lewis, A., V. Jogini, …, B. Roux. 2008. Atomic constraints between the voltage sensor and the pore domain in a voltage-gated K$^+$ channel of known structure. *J. Gen. Physiol.* 131:549–561.

15. Weiss, H. J. 1975. Platelet physiology and abnormalities of platelet function (second of two parts). *N. Engl. J. Med.* 293:580–588.

16. McEver, R. P. 2001. Adhesive interactions of leukocytes, platelets, and the vessel wall during hemostasis and inflammation. *Thromb. Haemost.* 86:746–756.

17. Savage, B., E. Saldívar, and Z. M. Ruggeri. 1996. Initiation of platelet adhesion by arrest onto fibrinogen or translocation on von Willebrand factor. *Cell.* 84:289–297.

18. Andrews, R. K., J. A. López, and M. C. Berndt. 1997. Molecular mechanisms of platelet adhesion and activation. *Int. J. Biochem. Cell Biol.* 29:91–105.

19. Matsushita, T., and J. E. Sadler. 1995. Identification of amino acid residues essential for von Willebrand factor binding to platelet glycoprotein Ib. Charged-to-alanine scanning mutagenesis of the A1 domain of human von Willebrand factor. *J. Biol. Chem.* 270:13406–13414.

20. Cauwenberghs, N., K. Vanhoorelbeke, …, H. Deckmyn. 2001. Epitope mapping of inhibitory antibodies against platelet glycoprotein Ibα reveals interaction between the leucine-rich repeat N-terminal and C-terminal flanking domains of glycoprotein Ibα. *Blood.* 98:652–660.

21. Dumas, J. J., R. Kumar, …, L. Mosyak. 2004. Crystal structure of the wild-type von Willebrand factor A1-glycoprotein Ibα complex reveals conformation differences with a complex bearing von Willebrand disease mutations. *J. Biol. Chem.* 279:23327–23334.

22. Varughese, K. I., Z. M. Ruggeri, and R. Celikel. 2004. Platinum-induced space-group transformation in crystals of the platelet glycoprotein Ib α N-terminal domain. *Acta Crystallogr. D Biol. Crystallogr.* 60:405–411.

23. Huizinga, E. G., S. Tsuji, …, P. Gros. 2002. Structures of glycoprotein Ibα and its complex with von Willebrand factor A1 domain. *Science.* 297:1176–1179.

24. Lou, J., and C. Zhu. 2008. Flow induces loop-to-β-hairpin transition on the β-switch of platelet glycoprotein Ibα. *Proc. Natl. Acad. Sci. USA.* 105:13847–13852.

25. Lu, D., A. Aksimentiev, …, K. Schulten. 2006. The role of molecular modeling in bionanotechnology. *Phys. Biol.* 3:S40–S53.

26. Lee, E. H., J. Hsin, …, K. Schulten. 2009. Discovery through the computational microscope. *Structure.* 17:1295–1306.

27. Sotomayor, M., and K. Schulten. 2007. Single-molecule experiments in vitro and in silico. *Science.* 316:1144–1148.

28. Chen, Z., J. Lou, …, K. Schulten. 2008. Flow-induced structural transition in the β-switch region of glycoprotein Ib. *Biophys. J.* 95:1303–1313.

29. Dinner, A. R., T. Lazaridis, and M. Karplus. 1999. Understanding β-hairpin formation. *Proc. Natl. Acad. Sci. USA.* 96:9068–9073.

30. Muñoz, V., E. R. Henry, …, W. A. Eaton. 1998. A statistical mechanical model for β-hairpin kinetics. *Proc. Natl. Acad. Sci. USA.* 95: 5872–5879.

31. Du, D., Y. Zhu, …, F. Gai. 2004. Understanding the key factors that control the rate of β-hairpin folding. *Proc. Natl. Acad. Sci. USA.* 101:15915–15920.

32. Kuo, N. N.-W., J. J.-T. Huang, …, S. I. Chan. 2005. Effects of turn stability on the kinetics of refolding of a hairpin in a β-sheet. *J. Am. Chem. Soc.* 127:16945–16954.

33. Bonomi, M., D. Branduardi, …, M. Parrinello. 2008. The unfolded ensemble and folding mechanism of the C-terminal GB1 β-hairpin. *J. Am. Chem. Soc.* 130:13938–13944.

34. Juraszek, J., and P. G. Bolhuis. 2009. Effects of a mutation on the folding mechanism of a β-hairpin. *J. Phys. Chem. B.* 113:16184–16196.

35. Thukral, L., J. C. Smith, and I. Daidone. 2009. Common folding mechanism of a β-hairpin peptide via non-native turn formation revealed by unbiased molecular dynamics simulations. *J. Am. Chem. Soc.* 131:18147–18152.

36. Lewandowska, A., S. Ołdziej, …, H. A. Scheraga. 2010. Mechanism of formation of the C-terminal β-hairpin of the B3 domain of the immunoglobulin-binding protein G from *Streptococcus*. IV. Implication for the mechanism of folding of the parent protein. *Biopolymers.* 93:469–480.

37. Darve, E., D. Wilson, and A. Pohorille. 2002. Calculating free energies using a scaled-force molecular dynamics algorithm. *Mol. Simul.* 28:113–144.

38. Hénin, J., and C. Chipot. 2004. Overcoming free energy barriers using unconstrained molecular dynamics simulations. *J. Chem. Phys.* 121:2904–2914.

39. Chipot, C., and A. Pohorille. 2007. Free Energy Calculations: Theory and Applications in Chemistry and Biology. Springer, NY.

40. Humphrey, W., A. Dalke, and K. Schulten. 1996. VMD: visual molecular dynamics. *J. Mol. Graph.* 14:33–38, 27–28.

41. MacKerell, Jr., A., D. Bashford, …, M. Karplus. 1998. All-atom empirical potential for molecular modeling and dynamics studies of proteins. *J. Phys. Chem. B.* 102:3586–3616.

42. Phillips, J. C., R. Braun, …, K. Schulten. 2005. Scalable molecular dynamics with NAMD. *J. Comput. Chem.* 26:1781–1802.

43. Jorgensen, W. L., J. Chandrasekhar, …, M. L. Klein. 1983. Comparison of simple potential functions for simulating liquid water. *J. Chem. Phys.* 79:926–935.

44. Martyna, G. J., D. J. Tobias, and M. L. Klein. 1994. Constant pressure molecular dynamics algorithms. *J. Chem. Phys.* 101:4177–4189.

45. Kolinski, A., and J. Skolnick. 1994. Monte Carlo simulations of protein folding. I. Lattice model and interaction scheme. *Proteins: Struct. Funct. Gen.* 18:338–352.

46. Şali, A., E. Shakhnovich, and M. Karplus. 1994. Kinetics of protein folding: a lattice model study of the requirements for folding to the native state. *J. Mol. Biol.* 235:1614–1636.

47. Metropolis, N., A. W. Rosenbluth, …, E. Teller. 1953. Equation of state calculations by fast computing machines. *J. Chem. Phys.* 21:1087–1092.

48. Flory, P. J. 1992. Principles of Polymer Chemistry. Cornell University Press, Ithaca, NY.

49. Perkins, T. T., D. E. Smith, and S. Chu. 1997. Single polymer dynamics in an elongational flow. *Science.* 276:2016–2021.

50. Zhang, X., K. Halvorsen, …, T. A. Springer. 2009. Mechanoenzymatic cleavage of the ultralarge vascular protein von Willebrand factor. *Science.* 324:1330–1334.